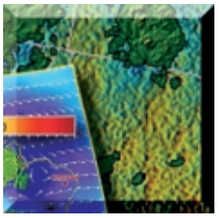

Estimating Oceanic Mixed-Layer Depth from Internal Wave Evolution Observed from Radarsat-1 SAR

Xiaofeng Li, Pablo Clemente-Colón, and Karen S. Friedman

One Radarsat-1 SAR image acquired on 31 July 1998 was used to study internal wave characteristics off the northeastern coast of the United States. The image showed several trains of internal waves, with several wave packets in each train. By assuming that the local semidiurnal tide period is the generating source for these waves, and by measuring the distance between the wave packets, we were able to derive the group velocity of the internal waves from synthetic aperture radar (SAR) images directly. If we also assume that the ocean is a two-layer finite depth model, we can then derive the mixed-layer depth by matching the group velocity measured from the SAR image with that simulated by the model. Results show reasonably good agreement between *in situ* conductivity-temperature-depth data and expendable bathythermographic climatology measurements. (Keywords: Internal wave, SAR, Two-layer model.)

INTRODUCTION

Oceanic internal waves are frequently observed on the continental shelf during the summer season, when the ocean is stratified. These waves, usually generated at the tidal frequency, propagate along the density interface as highly coherent packets, each having several wave crests. The upper mixed layer is usually of the order of a few tens of meters thick during the summer. When internal wave amplitudes are large, the local sea surface roughness is modulated by (1) the hydrodynamic variation of surface waves due to the internal wave orbital velocity and/or (2) wave damping by surface films due to surface convergence and divergence in the internal wave field.[1,2] In addition, oceanic internal waves have wavelengths on the order of a few hundred meters, with the internal wave packets being separated by several kilometers. Since the internal waves modulate the sea surface roughness field, they can be imaged by synthetic aperture radar (SAR) through the mechanism of resonant or Bragg scattering over an incidence angle range of 20 to 70°.

Internal waves have been detected in SAR images since the early 1980s.[1–8] The remote sensing of ocean features with SAR depends on the interaction of microwaves and short ocean waves. As described in a review by Valenzuela,[9] experimental studies have established resonant or Bragg scattering as the most important mechanism in the interaction of an electromagnetic wave (e.g., a radar pulse) and the ocean surface.

Intensity variations in SAR imagery result from variations in the amount of radiation backscattered by the dynamic ocean surface. In a Georgia Strait experiment, Hughes and Gower[4] used airborne SAR to obtain quantitative measurements of surface wave modulations induced by natural and ship-generated internal waves, including the determination of the phase relationship between SAR image roughness variations and internal wave amplitude. In a SAR internal wave signature experiment by Gasparovic et al.,[10] repeated aircraft passes were used to observe the propagation of internal waves in the Middle Atlantic Bight. The waves were registered to the known position of a research vessel in the image, and the offsets were used to calculate the propagation velocity of the internal waves. These two studies verified that sea surface manifestations of internal wave fields could be observed by SAR technology.

More recently, Liu et al.[8] studied the nonlinear internal wave evolution in the East and South China Seas with European Remote Sensing satellite (ERS-1) SAR images. Porter and Thompson[11] used the internal wave parameters measured from ERS-1 SAR to estimate the structure of the shelf water column. These studies showed that the oceanic interior structure could be estimated via remote sensing techniques.

RADARSAT-1 SAR DATA COLLECTION

Data for the study reported in this article were obtained in the Middle Atlantic Bight (Fig. 1). One Radarsat-1 standard mode SAR image, taken at 2240:41 GMT on 31 July 1998, was used. Four subimages containing internal wave signatures (boxes labeled I–IV in Fig. 1) are enlarged in Fig. 2.

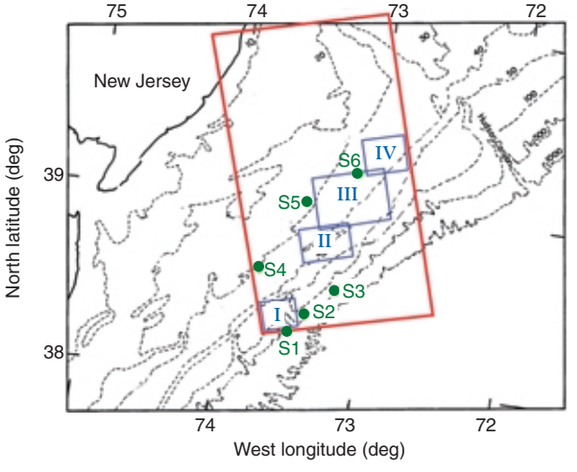

Figure 1. The location and bathymetry (in meters) of the Middle Atlantic Bight. The red box encompasses the Radarsat-1 SAR image coverage areas. Four subimages (I–IV) and six conductivity-temperature-depth stations (S1–6) are indicated.

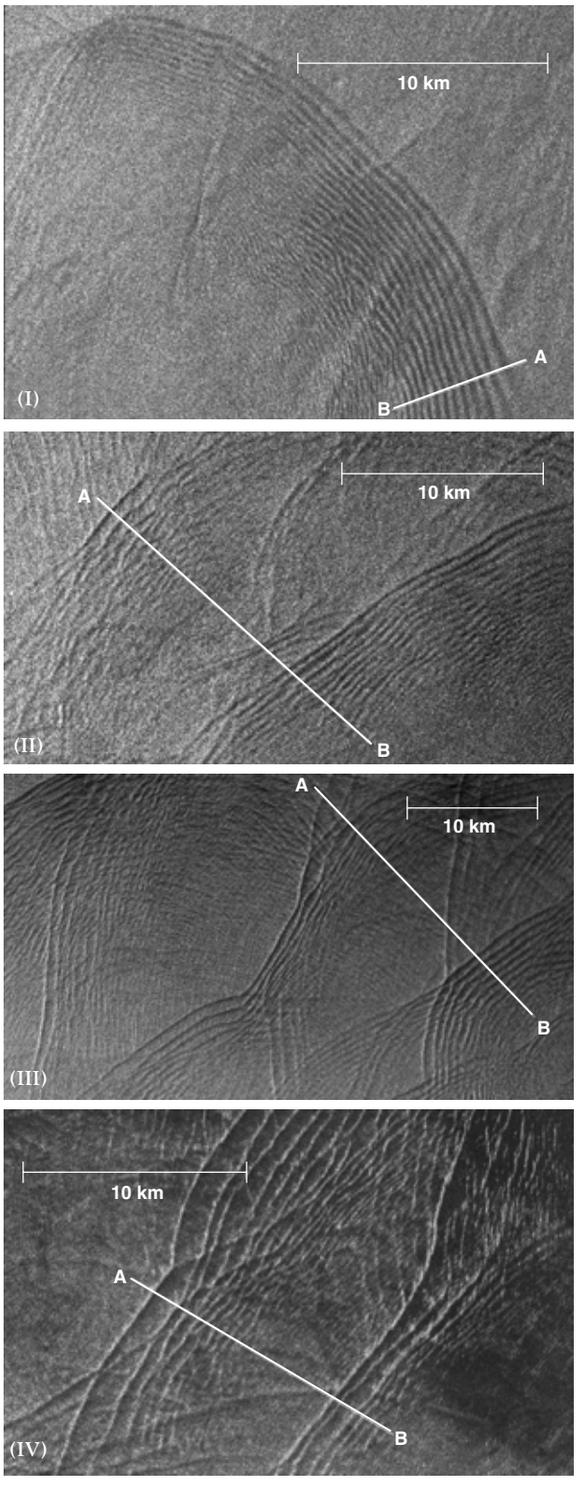

Figure 2. Enlargements of SAR image areas I–IV shown in Fig. 1. Strong internal wave signatures are seen as alternating dark and bright lines. Sampling profiles of Fig. 3 were taken from points A to B. The images were obtained at 2240:41 GMT on 31 July 1998 (original image resolution = 25 m, swath width = 100 km). (© Canadian Space Agency, 1998.)

The Canadian Radarsat-1 SAR operates at C band (5.3-GHz frequency, 5.6-cm wavelength) and horizontal polarization. Its standard beam mode has a swath width of 100 km and a spatial resolution of 25 m (pixel spacing of 12.5 m). One can observe many internal wave packets in a single standard mode image. In this study, we focused on three pairs of well-defined internal wave packets shown for subimages II, III, and IV (see Figs. 2b–2d). Information derived from the SAR images is given in Table 1.

The pixel values along the lines overlaid on subimages I through IV were plotted in Fig. 3. From this figure we can calculate the average internal wave wavelength from the first few big wave crests. The number of dominant wave crests used in calculating average wavelength is given in Table 1.

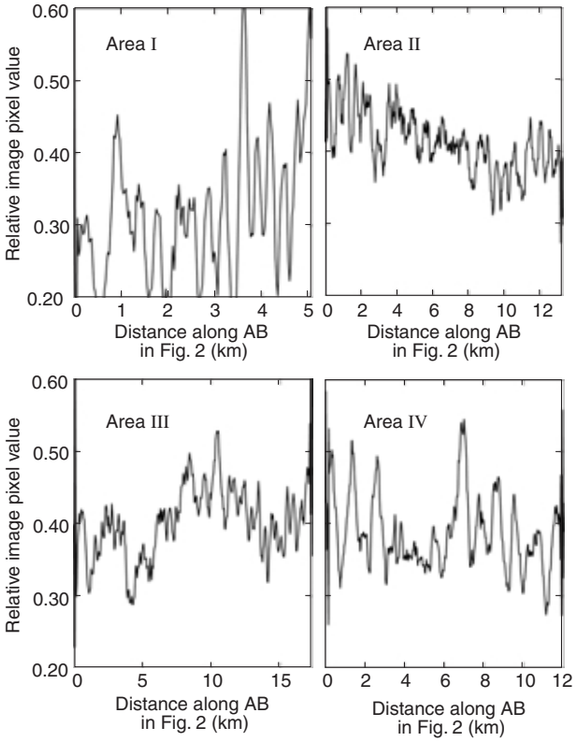

Figure 3. The four sampling profiles across the middle of the internal waves along lines AB shown in Fig. 2.

IN SITU MEASUREMENT DATA

Since no simultaneous field measurement data were available to us in this area, we searched the newly released Global Ocean Observation Database (GOODBase II) provided by Scripps Institute of Oceanography and the National Oceanic and Atmospheric Administration (NOAA). GOODBase II covers data from around the world from 1874 to 1996, with 5.4 million stations and 13.8 million parameter profiles. Mechanical conductivity-temperature-depth (CTD) data are also available from GOODBase II. The new GOODBase provides online access (http://oceans.ucsd.edu/goodbase/) to subsets of these ocean profile data, selected by geographical region, date range, season, etc.

We searched the CTD data in GOODBase II for the 1990s and found six measurement stations (S1–6 in Fig. 1a) in the vicinity of our internal wave study region for the same month, but in 1995. Figure 4 shows the density profiles calculated from temperature–salinity profiles measured at these stations from 14–18 July 1995.

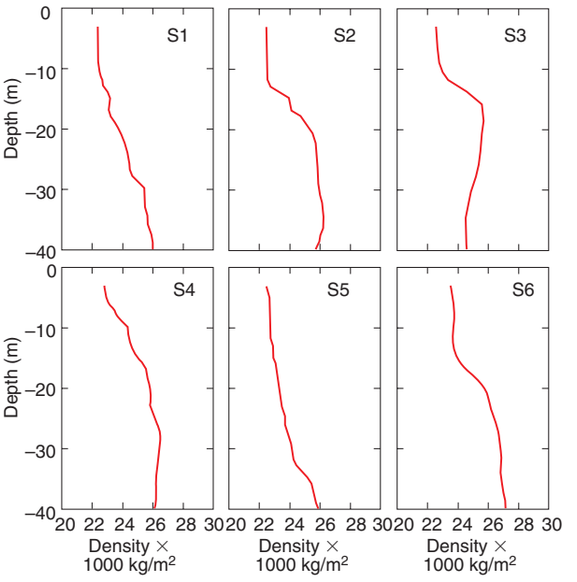

Figure 4. Conductivity-temperature-depth profiles at stations S1–S6.

Table 1. Internal wave parameters measured from the SAR image.

Sub-image	Packets	D (km)	Average wavelength per packet, λ (m)		Number of dominant wave crests per packet		Group velocity of internal wave packet, C_g (m/s)	Period of local semidiurnal tide, T (h:min)	Water depth (m)
			1	2	1	2			
I	1	N/A	410	N/A	11	N/A	N/A	12:40	100
II	2	11.2	560	580	6	11	0.25	12:40	50
III	2	13.8	560	780	7	9	0.30	12:40	35
IV	2	9.5	630	760	9	7	0.21	12:40	35

Note: D = average distance between the leading wave crest of different groups of internal wave packets.

The R/V *Pelican* of the NOAA National Marine Fisheries Service provided these cruise measurements. These profiles clearly show that a thin oceanic upper mixed layer existed above the permanent thermocline. The mixed-layer depth was between 10 and 13 m on the continental shelf. In addition, Fig. 5 shows the climatology of mixed-layer depth derived from expendable bathythermographic (XBT) data for July and August. The contours were derived at the University of Delaware from *in situ* measurement data over a 10-year period (1980s). Zheng et al.[12] first used these climatology data to estimate the mixed-layer evolution during the summer months in the Middle Atlantic Bight for their internal wave study. Although it would be ideal to have simultaneous ground truth measurements, Zheng et al. showed that the XBT climatology of estimated mixed-layer depth can be used to derive the representative mixed-layer depth at a later time. They also showed that the mixed-layer depth can vary as much as 1 m for every 10-day period in the Middle Atlantic Bight.

Our SAR image was taken on 31 July 1998, so the error should be within 2 m. The estimated mixed-layer depth was not used in our dynamical analysis model as an input parameter; rather, we used it for validation purposes. From Fig. 5 one can see that, in the internal wave evolution region, the mixed-layer depth is about 9.0 m. From the previous CTD and XBT climatology data, it is reasonable to estimate that the oceanic mixed layer is on the order of 10 m, with variations of 2 m. This value was used as ground truth to test a two-layer model.

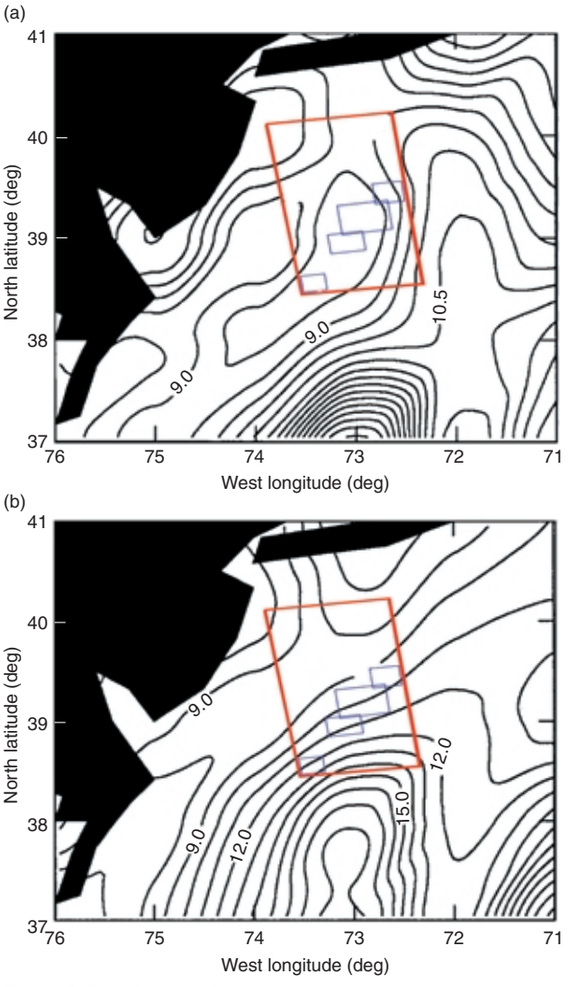

Figure 5. Climatology of the oceanic mixed-layer depth (in meters) in the Middle Atlantic Bight derived from XBT data for (a) July and (b) August. Red overlays show SAR image coverage as in Fig. 1.

TWO-LAYER FINITE DEPTH MODEL

To understand the dynamics of these internal waves observed in the SAR image, we used a two-layer ocean model to simulate internal wave propagation. If we assume (1) the Boussinesq approximation, (2) incompressible flow, (3) no shear, and (4) negligible Earth rotation effects, then the vertical momentum equation used to describe the small-amplitude vertical motion in a stratified ocean of an arbitrary Brunt–Väisälä frequency, $N(z)$, can be written[13] as

$$\frac{\partial^2}{\partial t^2}(\nabla^2 W) + N^2(z)\nabla_h^2 W = 0, \tag{1}$$

where W is the amplitude of the vertical velocity and the subscript h indicates a gradient in the horizontal direction. The wave solutions, which are periodic in $\boldsymbol{x}$ and t, can be sought in the form

$$W(\boldsymbol{x}, z, t) = W(z)e^{i[kx-\sigma(k)t]}.$$

The x axis is chosen to be perpendicular to the wave crest. In this case, the internal wave propagation direction is perpendicular to the local bathymetry. Following Phillips,[13] by substituting W into the governing Eq. 1, we have

$$\frac{d^2W(z)}{dz^2} + \left[\frac{N^2(z)}{\sigma^2} - 1\right]k^2 W(z) = 0, \tag{2}$$

where $N(z)$ is expressed as

$$N(z) = \left(-\frac{g}{\rho}\frac{\partial \rho}{\partial z}\right)^{1/2}, \tag{3}$$

and

σ = the internal wave frequency,

$k = 2\pi/\lambda$ is the horizontal wavenumber,

ρ = the water density, and

g = the acceleration of gravity.

Equation 2 is solved analytically. The water density changes rapidly within a small depth range (Δd) around the pycnocline. Therefore, the Brunt–Väisälä frequency $N(z)$ is at maximum value near the thermocline and is small at other depths. We can thus assume that the ocean is a two-layer system having an upper mixed layer with depth h_1 and total depth H. The boundary conditions at the surface and bottom are $W(0) = 0$ and $W(-H) = 0$, respectively. As an internal boundary condition across the thermocline, the vertical velocity of the lowest internal wave mode is continuous. We therefore have $W(-h_1) = W(-h_1 - \Delta d)$.

Equation 2, together with these boundary conditions, forms a second-order Sturm–Liouville problem. The lowest eigenvalue satisfying the governing equation and boundary conditions leads to the dominant internal wave mode dispersion relation[13]

$$\sigma = \left[\frac{k \cdot g'}{k \cdot \Delta d + \coth(k \cdot h_1) + \coth(k \cdot h_2)} \right]^{1/2}, \qquad (4)$$

where g' is the reduced gravity associated with the density change across the thermocline interface given by $g' = g\Delta\rho/\rho$, g is taken as 9.8 m/s^2, and h_1 and h_2 are the water depths of the upper and lower layer ($H = h_1 + h_2$), respectively.

The wavelength λ of the internal waves, as determined from the SAR observations, is much greater than Δd, so that $k\Delta d << 1$. Therefore, this term can be neglected in Eq. 4. The wavenumber $k = (2\pi/\lambda)$ is then calculated. The phase velocity C_p can be obtained from the phase speed definition for any wave by

$$C_p = \sigma/k\,. \qquad (5)$$

From Eq. 4, after neglecting the $k\Delta d$ term, the group velocity C_g is

$$C_g = \frac{\partial \sigma}{\partial k} = C_p \left[\frac{1}{2} + \frac{k \cdot h_1 \cdot \sinh^2(k \cdot h_2) + k \cdot h_2 \cdot \sinh^2(k \cdot h_1)}{2 \sinh(k \cdot h_1) \cdot \sinh k(h_1 + h_2) \cdot \sinh(k \cdot h_2)} \right]. \qquad (6)$$

In this case, $C_p \gtrsim C_g$.

RESULTS

We used the following input parameters to run the two-layer model: internal wave wavelengths, which were measured from the SAR image and given in Table 1; and, based on the temperature–salinity profiles, the reduced gravity calculated as 1×10^{-3} for shelf waters. (This is a typical number for the area.[12]) The topography contours are shown in Fig. 1a. We used a water depth value of 50 m for internal wave packets in Fig. 2b (λ = 580 m) and 35 m for those packets in Figs. 2c and 2d (λ = 780 m). Substituting these numbers into the governing equations, the internal wave group velocity was plotted as a function of oceanic mixed-layer depth in Fig. 6.

The measured group velocities from the SAR image are given in Table 1. By matching the group velocities simulated from the two-layer model and those estimated from the SAR image, one can find the corresponding mixed-layer depth for the special group velocity using the curves in Fig. 6. In this case, the estimated mixed-layer depth was between 8 and 11 m, with a mean value of 9.5 m. This value is in very good agreement with that obtained from historic XBT measurements. Although the estimated mixed-layer depth is slightly smaller than the 1995 cruise measurement, the error is less than 10%.

Using Eq. 5, we can also obtain the phase velocity C_p. In this case, C_g was between 0.97 and 0.99 C_p. We can see that the group velocity of the internal wave packets is less than the phase velocity. Therefore, these groups of internal waves are dispersive. The wave energy dissipates with time. This observation is consistent with earlier ones.[1,13,14] Here, since C_g is very close to C_p, the dissipation is a long process.

Based on soliton theory, Zheng et al.[12] derived the period T_g of a wave packet for a sloping bottom:

$$T_g = \int_0^{\lambda_g} \frac{dx}{C_g} = \frac{1}{C_g} \frac{4H^2}{h_1 \tan(\theta)} \times \left[\ln\left(1 - \frac{h_1}{2H} + \frac{h_1 \lambda_g}{4H^2} \tan(\theta)\right) - \ln\left(1 - \frac{h_1}{2H}\right) \right], \qquad (7)$$

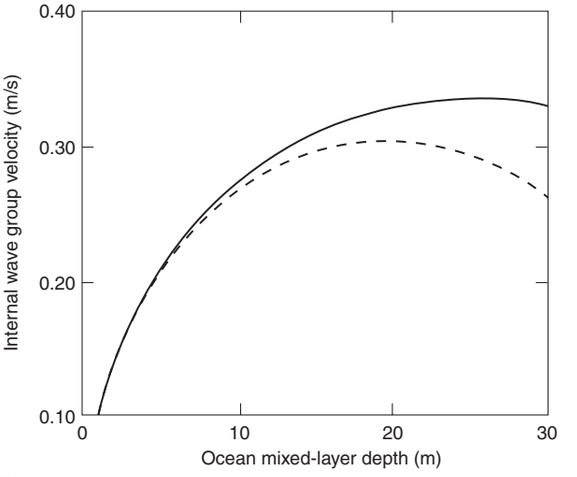

Figure 6. Internal wave group velocity versus oceanic mixed-layer depth as simulated by a two-layer finite depth model with a relative density difference of 0.001 (water depth of solid curve, 50 m; dashed curve, 35 m).

where the total water depth H is 50 m and the mixed-layer depth h_1 is 9.5 m. In the Middle Atlantic Bight, the slope $\tan(\theta) = 3.2 \times 10^{-3}$. In this case, C_g is found to be about 0.25 m/s and $\lambda_g = 11$ km. Therefore, all the parameters in Eq. 7 are known. T_g was found to be about 13 h, which coincides with the period of the local semidiurnal tide (12 h, 40 min), thus confirming that the local semidiurnal tide is the main generating source for the internal wave packets observed in the Radarsat SAR image.

CONCLUSION

Radarsat-1 SAR imagery provides wide coverage over the ocean. In this study, a Radarsat-1 SAR standard mode image, acquired on 31 July 1998, was processed and interpreted. We analyzed three pairs of continental shelf internal waves in the Middle Atlantic Bight. We assumed that the ocean is a two-layer system, and that the local semidiurnal tide is the generating force for the internal waves. We could then estimate the mixed-layer depth by matching the measured internal wave group velocity with that calculated with the two-layer model. Here, a practical model was established to estimate the oceanic mixed-layer depth based on internal wave characteristics in the Middle Atlantic Bight in the summer. The resulting estimate was in good agreement with cruise measurements on the continental shelf and the climatology of historic XBT measurements.

REFERENCES

[1] Alpers, W., and Salusti, E., "Scylla and Charybdis Observed from Space," *J. Geophys. Res.* **88**, 1800–1808 (1983).

[2] Silva, J. C. D., Jeans, D. R. G., Robinson, I. S., and Sherwin, T., "The Application of Near Real-Time ERS-1 SAR Data to the Prediction of the Location of Internal Waves at Sea," *Int. J. Remote Sens.* **18**(16), 3507–3517 (1997).

[3] Osborne, A. R., and Burch, T. L., "Internal Solitons in the Andaman Sea," *Science* **208**, 451–460 (1980).

[4] Hughes, B. A., and Gower, J. F. R., "SAR Imagery and Surface Truth Comparisons of Internal Waves in Georgia Strait, British Columbia, Canada," *J. Geophys. Res.* **88**, 1809–1824 (1983).

[5] Kasischke, E. S., Tseng, Y. C., Meadows, G. A., and Liu, A. K., "Observations of Internal Waves and Frontal Boundaries on SEASAT SAR Imagery Collected over the Eastern North Atlantic Ocean," in *Proc. 17th Int. Symp. on Remote Sensing of the Environment*, Ann Arbor, MI, pp. 1193–1210 (1983).

[6] Gasparovic, R. F., Apel, J. R., Thompson, D. R., and Tochko, J. S., "A Comparison of SIR-B Synthetic Aperture Radar Data with Ocean Internal Wave Measurements," *Science* **232**, 1529–1531 (1986).

[7] Liu, A. K., "Analysis of Nonlinear Internal Waves in the New York Bight," *J. Geophys. Res.* **93**, 12,317–12,329 (1988).

[8] Liu, A. K., Chang, Y. S., Hsu, M. K., and Liang, N. K., "Evolution of Nonlinear Internal Waves in the East and South China Seas," *J. Geophys. Res.* **103**, 7995–8008 (1998).

[9] Valenzuela, R. G., "Theories for the Interaction of Electromagnetic and Ocean Waves—A Review," *Boundary Layer Meteorol.* **13**, 61–85 (1978).

[10] Gasparovic, R. F., Apel, J. R., and Kasischke, E. S., "An Overview of the SAR Internal Wave Signature Experiment," *J. Geophys. Res.* **10**, 12,304–12,316 (1988).

[11] Porter, D. J., and Thompson, D. R., "Continental Shelf Parameters Inferred from SAR Internal Wave Observations," *J. Atmos. Oceanic Technol.* **16**, 475–487 (1999).

[12] Zheng, Q., Yan, X. H., and Klemas, V., "Statistical and Dynamical Analysis of Internal Waves on the Continental Shelf of the Middle Atlantic Bight from Space Shuttle Photographs," *J. Geophys. Res.* **98**, 8495–8504 (1993).

[13] Phillips, O. M., *The Dynamics of the Upper Ocean*, 2nd Ed., Cambridge University Press, New York (1977).

[14] Etkin, V. S., and Smirnov, A. V., "Observations of Internal Waves in the Ocean by Radar Methods," in *Proc. Int. Geoscience and Remote Sensing*, Vol. 1, pp. 143–145 (1992).

ACKNOWLEDGMENTS: This research was funded by the NOAA/NESDIS Ocean Remote Sensing Program as part of the NESDIS Monitoring and Detection Project (NEMoDe). Radarsat data were obtained under NASA Radarsat ADRO Project #396 and processed by the Alaska SAR facility. The climatology XBT data were kindly provided by Dr. Quanan Zheng from the University of Delaware. We would like to thank three reviewers for their valuable comments.

THE AUTHORS

XIAOFENG LI is affiliated with NOAA/NESDIS. His e-mail address is xiaofeng.li@noaa.gov.

PABLO CLEMENTE-COLÓN is affiliated with the NOAA/NESDIS Office of Research and Applications. His e-mail address is pablo.clemente-colon@noaa.gov.

KAREN S. FRIEDMAN is affiliated with NOAA/NESDIS. Her e-mail address is kfriedman@nesdis.noaa.gov.